Cancer Research

Epithelial-to-Mesenchymal Transition Promotes Tubulin Detyrosination and Microtentacles that Enhance Endothelial Engagement

Rebecca A. Whipple[1], Michael A. Matrone[1,2], Edward H. Cho[1,2], Eric M. Balzer[1,2], Michele I. Vitolo[1], Jennifer R. Yoon[1,2], Olga B. Ioffe[1,4], Kimberly C. Tuttle[1,4], Jing Yang[5], and Stuart S. Martin[1,2,3]

Abstract

Epithelial-to-mesenchymal transition (EMT) is associated with increased breast tumor metastasis; however, the specific mechanisms by which EMT promotes metastasis remain somewhat unclear. Despite the importance of cytoskeletal dynamics during both EMT and metastasis, very few current studies examine the cytoskeleton of detached and circulating tumor cells. Specific posttranslational α-tubulin modifications are critical for adherent cell motility and implicated in numerous pathologies, but also remain understudied in detached cells. We report here that EMT induced through ectopic expression of Twist or Snail promotes α-tubulin detyrosination and the formation of tubulin-based microtentacles in detached HMLEs. Mechanistically, EMT downregulates the tubulin tyrosine ligase enzyme, resulting in an accumulation of detyrosinated α-tubulin (Glu-tubulin), and increases microtentacles that penetrate endothelial layers to facilitate tumor cell reattachment. Confocal microscopy shows that microtentacles are capable of penetrating the junctions between endothelial cells. Suppression of endogenous Twist in metastatic human breast tumor cells is capable of reducing both tubulin detyrosination and microtentacles. Clinical breast tumor samples display high concordance between Glu-tubulin and Twist expression levels, emphasizing the coupling between EMT and tubulin detyrosination *in vivo*. Coordinated elevation of Twist and Glu-tubulin at invasive tumor fronts, particularly within ductal carcinoma *in situ* samples, establishes that EMT-induced tubulin detyrosination occurs at the earliest stages of tumor invasion. These data support a novel model where the EMT that occurs during tumor invasion downregulates tubulin tyrosine ligase, increasing α-tubulin detyrosination and promoting microtentacles that could enhance the reattachment of circulating tumor cells to the vascular endothelium during metastasis. *Cancer Res; 70(20); 8127–37. ©2010 AACR.*

Introduction

During metastasis, tumor cells respond to the changing microenvironment with internal adaptations that are reflected in the cytoskeleton. Investigating how cytoskeletal alterations provide selective advantages to tumor cells could identify new therapeutic targets to reduce metastasis. Recently, attention has focused on the complex transition that differentiated epithelial cells undergo into a mesenchymal state and its involvement in tumor progression (1–3). Activation of this epithelial-to-mesenchymal transition (EMT) has been implicated as a means by which cancer cells can overcome the physical constraints of the primary tumor to become motile, invade surrounding tissue, and enter the vasculature (3, 4). It is also worth considering whether the molecular programs that tumor cells execute in response to the changing microenvironment could influence the metastatic potential of circulating tumor cells (CTC).

Although there is significant research detailing the mechanisms involved with intravasation and the later stages of extravasation (5), the mechanism by which disseminated tumor cells reattach to the endothelium is poorly understood. Recent advances in intravital imaging have enabled direct observation and experimental manipulation of circulating cells *in vivo* (6, 7). Compelling intravital imaging shows that microtubule-destabilizing compounds prevent adhesion of circulating colon carcinoma cells to the vascular endothelium (8). Although the functional role of microtubules during initial tumor cell reattachment *in vivo* remains undetermined, we recently identified microtubule-based membrane protrusions (termed microtentacles) that frequently occur on detached breast carcinoma cell lines that exhibit mesenchymal phenotypes (9, 10). Microtentacles

Authors' Affiliations: [1]Marlene and Stewart Greenebaum National Cancer Institute Cancer Center, University of Maryland School of Medicine, Baltimore, Maryland; [2]Program in Molecular Medicine and Departments of [3]Physiology, [4]Pathology, and [5]Pharmacology and Pediatrics, School of Medicine, University of California, San Diego, La Jolla, California

Note: Supplementary data for this article are available at Cancer Research Online (http://cancerres.aacrjournals.org/).

Corresponding Author: Stuart S. Martin, University of Maryland School of Medicine, Room 10-29, Bressler Building, 655 West Baltimore Street, Baltimore, MD 21201. Phone: 410-706-6601; Fax: 410-706-6600; E-mail: ssmartin@som.umaryland.edu.

doi: 10.1158/0008-5472.CAN-09-4613

are supported by the mesenchymal-associated intermediate filament protein, vimentin, and also detyrosinated α-tubulin (Glu-tubulin), a posttranslational cleavage of the COOH-terminal tyrosine on α-tubulin (11). Stabilization of microtubules induces detyrosination that can inhibit microtubule disassembly (12), and detyrosinated microtubules can persist for as long as 16 hours in cells whereas dynamic tyrosinated microtubules typically persist for only 3 to 5 minutes (11). Restoration of the COOH-terminal tyrosine on α-tubulin is mediated by the tubulin tyrosine ligase (TTL) enzyme. Recent live-cell imaging in adherent fibroblasts show that most microtubules depolymerize upon contact with the cell membrane; however, microtubules in TTL knockout fibroblasts persist significantly longer at the membrane with an increased time spent growing (12). Interestingly, TTL suppression has been reported to provide a selective advantage during tumor growth (13), and the resulting tubulin detyrosination has been associated with poor prognosis in patients (14).

Membrane microtentacles in detached cells have been previously shown to be supported by detyrosinated microtubules in coordination with vimentin intermediate filaments (9, 10). These structural features, and the observation that microtentacles are strongly enhanced by actin-disrupting agents, establish microtentacles as novel cytoskeletal structures that are mechanistically distinct from traditional actin-based protrusions such as filopodia, invadopodia, and podosomes (15). Perturbation of microtentacles with tubulin-depolymerizing agents, vimentin-targeted phosphatase inhibitors, or expression of dominant-negative vimentin significantly reduces both the frequency of microtentacles and cellular reattachment to extracellular matrix (10, 16). Furthermore, microtubule- stabilizing compounds enhance adhesion and microtentacle frequency in detached breast carcinoma cells (17).

Given the increased microtentacle frequency in mesenchymal breast carcinoma cell lines, we chose to examine the incidence of microtentacles in immortalized human mammary epithelial cells (HMLE) that have undergone a regulated EMT through stable Twist or Snail expression (18, 19). Furthermore, we investigated the effects of suppressing endogenous Twist expression. We report here that EMT downregulates the expression of TTL enzyme in HMLEs, leading to elevated tubulin detyrosination and increased incidence of microtentacles. Suppression of endogenous Twist reduced the frequency of microtentacles and decreased the expression level and organization of Glu-tubulin. Moreover, a clear concordance between Twist expression and Glu-tubulin is observed in matched serial sections of patient tumors, reinforcing our observations *in vivo*. HMLE Twist and Snail lines attach at a significantly increased rate when suspended over a human bone marrow endothelial (HBME) layer, and confocal microscopy captures microtentacle extension to facilitate attachment and stabilization. Our results identify a novel regulatory mechanism within the EMT program that influences the posttranslational modification of α-tubulin, promoting microtentacle extension that enhances reattachment of breast tumor cells to endothelial cells.

Materials and Methods

Cell culture

HMLEs stably expressing green fluorescent protein (GFP), Twist, or Snail (20) were grown in MEGM medium kit (Lonza) at 37°C in 5% CO_2. MDA-MB-157 obtained from the American Type Culture Collection were maintained in L-15 (Gibco) containing 10% fetal bovine serum (FBS), penicillin-streptomycin (100 μg/mL), and L-glutamine (2 mmol/L) at 37°C without CO_2. HBME cells were provided by Antonio Passaniti (University of Maryland Greenebaum Cancer Center, Baltimore, MD) and grown in DMEM (Gibco) containing 10% FBS, penicillin-streptomycin (100 μg/mL each), and L-glutamine (2 mmol/L) at 37°C in 5% CO_2. Cell line authentication procedures are described in Supplementary Data.

Live cell imaging and microtentacle scoring

Live cell imaging and microtentacle scoring were previously described (10). Because the HMLE vector control is GFP+, we used CellMask-Orange membrane stain (Invitrogen) following the manufacturer's protocol. For each trial, at least 100 single cells were scored blindly for microtentacles after 30 minutes in suspension and counted positive when two or more protrusions extended greater than the radius of the cell body. Live cell imaging used an Olympus CKX41 inverted fluorescence microscope.

Indirect immunofluorescence

For suspended cell immunofluorescence, HMLE-GFP, Twist, and Snail cells were detached in serum-free medium for 30 minutes and fixed as previously described (10). For attached cell experiments, subconfluent HMLE-GFP, Twist, and Snail as well as MDA-MB-157 cells were fixed in 3.7% formaldehyde/PBS (10 minutes at room temperature).

Immunostaining used mouse monoclonal antibodies: vimentin clone V9 (1:1,000; Zymed) and twist1 (1:250; abCam), and rabbit polyclonal antidetyrosinated tubulin (Glu; 1:500; Chemicon). Secondary detection was with Alexa-568–conjugated anti-IgG and Hoescht-33342 (1:5,000; Sigma) for DNA.

Western blot

Subconfluent HMLE-GFP, Twist, Snail, and MDA-MB-157 were washed in PBS and harvested as previously described (10). Total protein (20 μg) was separated on a 4% to 12% NuPage MES Bis-Tris gradient gel (Invitrogen) then transferred to Immuno-Blot polyvinylidene difluoride membranes (Bio-Rad). Monoclonal E-cadherin (1:500; BD Biosciences), vimentin clone V9 (1:1,000; Zymed), twist1 (1:250; abCam), α-tubulin DM1A (1:2,000; Sigma), and β-actin (1:2,000; AC-15, Sigma). Polyclonal detyrosinated tubulin (1:1,000; Chemicon) and N-cadherin (1:500; Cell Signaling) and snail (1:250; Cell Signaling) were used. Secondary ECL+ chemiluminescent detection was used with horseradish peroxidase–conjugated anti-IgG antibodies (1:5,000; GE Healthcare). The rabbit polyclonal TTL antibody is described in Supplementary Methods.

Cell-electrode impedance attachment assay

Real-time, dynamic monitoring of cell substratum attachment was measured using the xCelligence RTCA-SP real-time

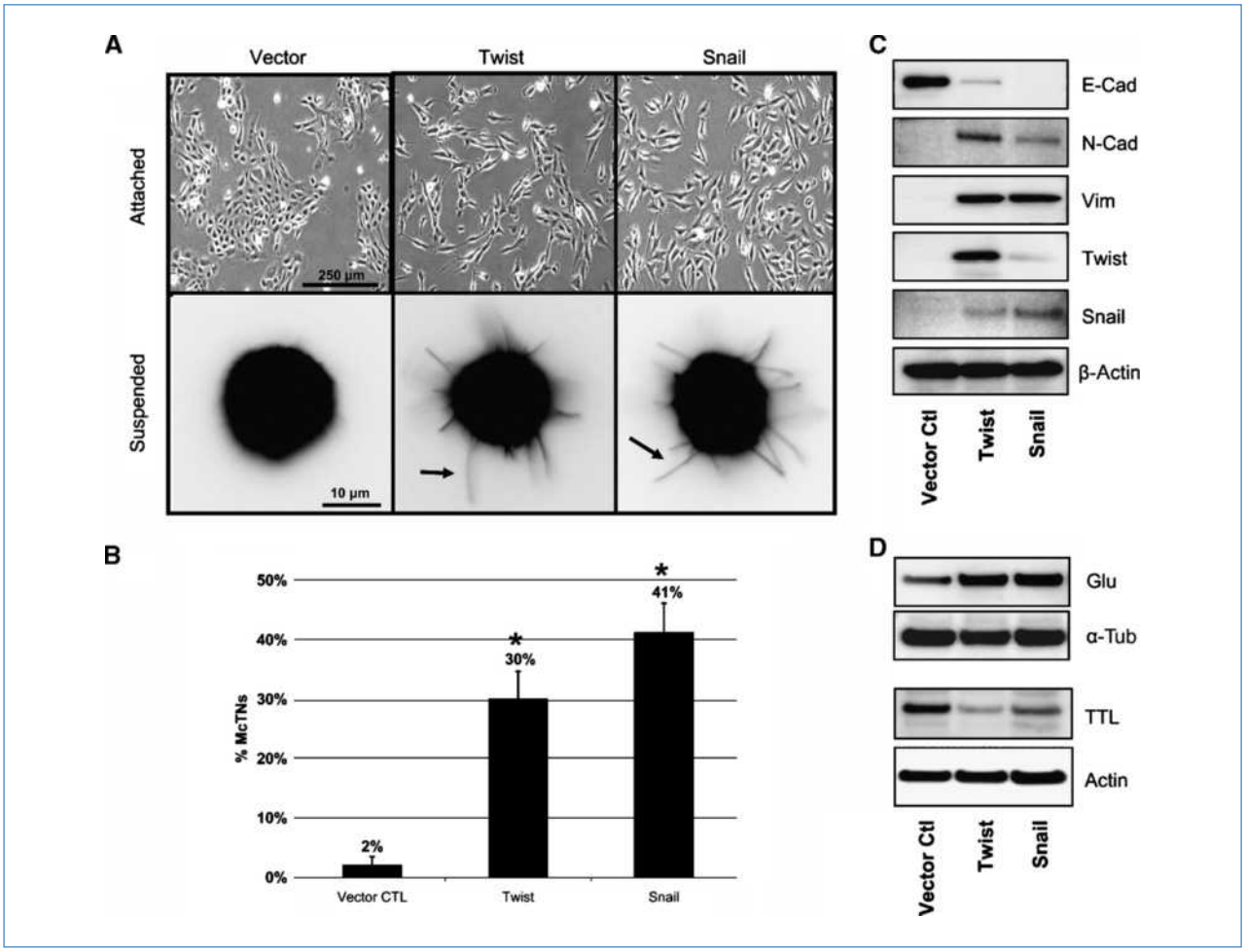

Figure 1. EMT promotes increased microtentacles and tubulin detyrosination in detached HMLEs. A, phase-contrast images of attached HMLE Twist and Snail cells compared with HMLE-GFP (top). Detached HMLE Twist and Snail display extensive membrane microtentacles (bottom, black arrows). B, populations of live, detached HMLE Twist and Snail cells display significantly higher microtentacle (McTNs) frequencies than HMLE-GFP cells. Columns, mean for six experiments, in which at least 100 CellMask-stained cells were counted; bars, SD ($P \leq 0.005$, *t* test, black asterisks). C, comparative expression profile of HMLE (GFP Vector Ctl, Twist, Snail), including E-cadherin, N-cadherin, vimentin (Vim), Twist, Snail, and β-actin as a loading control, showing mesenchymal hallmarks in Twist and Snail HMLEs. D, HMLE Twist and Snail have increased Glu-tubulin levels and decreased levels of TTL compared with the HMLE-GFP whereas total α-tubulin and actin are comparable.

cell sensing device (Roche) to compare the attachment rates of the HMLE GFP vector control, Twist, and Snail. HMLE cells (10,000) were seeded in triplicate into 96-well microelectronic sensored standard plates (E-plates). Attachment was expressed as a change in cell index, an arbitrary unit reflecting the relative change in electrical impedance from cell-electrode interaction across microelectronic sensor arrays. Electrical impedance was measured for 0.1 second every 5 minutes for 75 minutes. Values are the mean ± SD of triplicate wells (three independent trials).

HMLE attachment and microtentacle engagement to the HBME layer

HMLE-GFP, Twist, and Snail cell lines were stained with calcein-AM (0.5 μg/mL; Invitrogen). Cells were detached with enzyme-free cell dissociation solution, resuspended in growth medium, and 50,000 cells were plated over confluent HBME layers at 37°C. At 1 hour, the attached cells were washed with fresh growth medium. Fluorescence was measured using a Biotek SynergyHT microplate reader (excitation 485 nm, emission 528 nm). Attachment was calculated as the fluorescent signal after aspirating the medium divided by the fluorescent signal from duplicate wells that were not aspirated. Values shown are mean ± SD (eight independent trials). Confocal imaging is detailed in Supplementary Methods.

Patient samples and immunohistochemistry

Ten fresh/frozen patient breast tumor tissue samples obtained by surgery or biopsy from the UMGCC Pathology Biorepository and Research Core as well as a human breast cancer TMA (US BioMax) containing 33 cases of invasive ductal breast carcinoma and 13 cases of normal and nonmalignant breast tissue were examined. TMA sections were deparaffinized, rehydrated, and subjected to heat-induced

epitope retrieval (DakoTRS, S1699/1700), followed by endogenous peroxidase blocking with hydrogen peroxide. All sections were incubated with the primary antibody Twist (1:250; H-81, Santa Cruz) or detyrosinated tubulin (1:150; Chemicon) overnight. Diaminobenzidine detection was performed on an automatic stainer using EnVision+ (DAKO). The staining intensity of Twist and Glu-tubulin was scored independently and blindly for each section according to four categories: negative, 0; weak, 1; moderate, 2; and strong, 3. Samples with ±1 histologic scores and staining within matching cells were scored as "concordant." When staining intensity differed by at least two histologic scores (0–2 or 1–3) or within different cells, the sample was scored as "discordant" staining.

Results

Induction of EMT by Twist or Snail expression promotes microtentacle formation in detached HMLEs

To investigate the role that EMT plays in microtentacle formation in detached cells, HMLEs ectopically expressing the Twist or Snail transcription factors were analyzed and compared with a GFP-expressing vector control HMLE line. Adherent HMLE cells expressing Twist or Snail display a characteristic mesenchymal morphology compared with the vector control cells (Fig. 1A, top panels), including the loss of cell-cell contacts, cell scattering, and reduced apical-basal cell polarity (18, 19).

Given the morphologic alterations observed in adherent cells, we investigated the incidence of microtentacles in detached cells that have undergone EMT. HMLE cells were fluorescently labeled with CellMask. Following 30 minutes of suspension, HMLE Twist or Snail displayed extensive, motile microtentacles compared with the control cell line (Fig. 1A, bottom panels). Blinded quantitative analysis (Fig. 1B) revealed significantly higher microtentacle frequencies in the suspended HMLEs expressing Twist (15-fold) or Snail (20-fold) compared with the vector control cells ($P \leq 0.005$; $n = 6$, three independent trials).

Evaluation of hallmark EMT markers through Western blot supports the transition from epithelial to mesenchymal states. The protein expression profile illustrates E-cadherin to N-cadherin switch, vimentin expression, and both Twist and Snail upregulation in the respective transformed lines (Fig. 1C). Given the increased microtentacle frequency in HMLE lines that have transitioned to a mesenchymal state and our

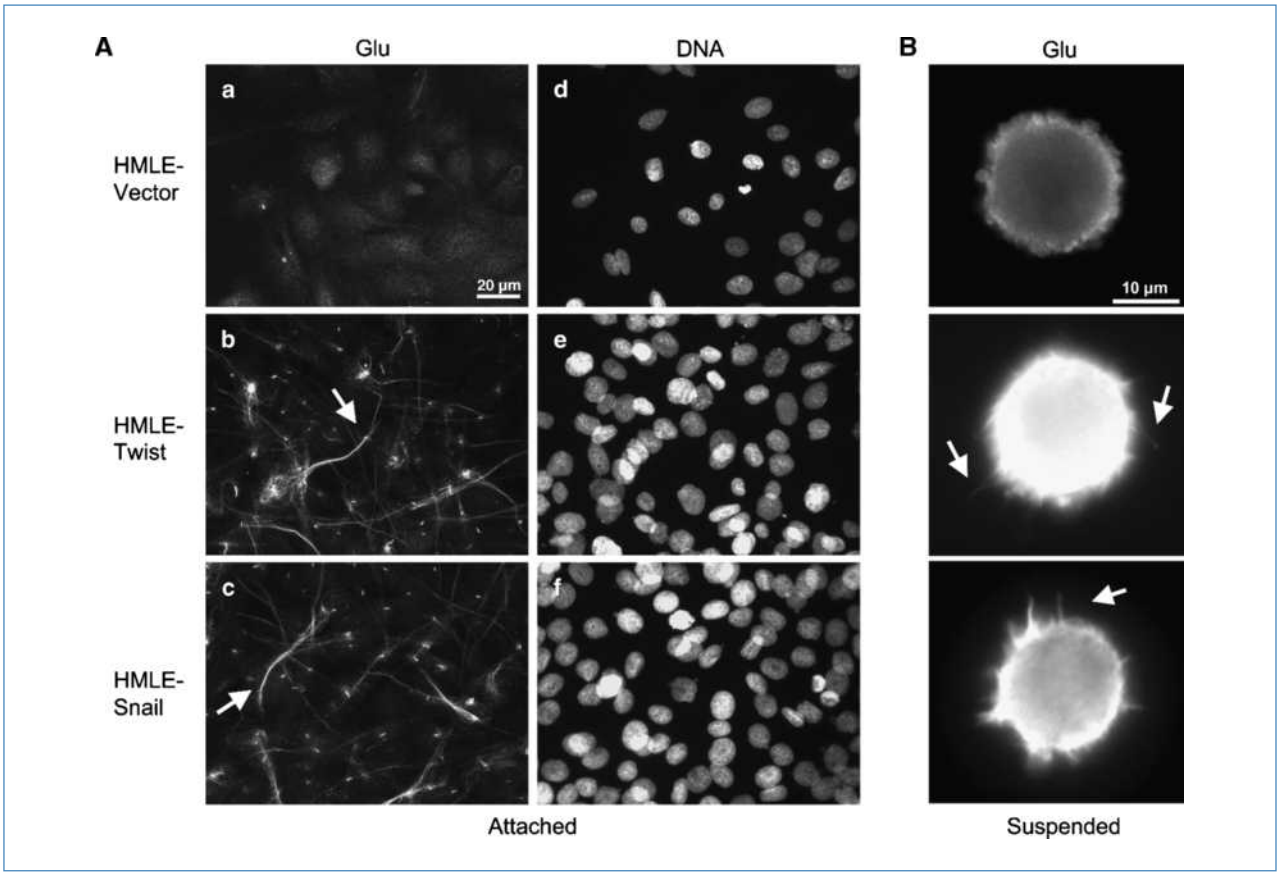

Figure 2. Glu-tubulin accumulation and reorganization during EMT. A, a–c, attached HMLE-GFP control shows weak Glu staining whereas the HMLE Twist and Snail display filamentous accumulation and bundling of Glu-tubulin (arrows). Hoescht (d–f) was used to visualize nuclei. B, detached cells were fixed and spun onto glass coverslips. Immunostaining indicates Glu-tubulin localization in HMLE Twist and Snail microtentacles (white arrows).

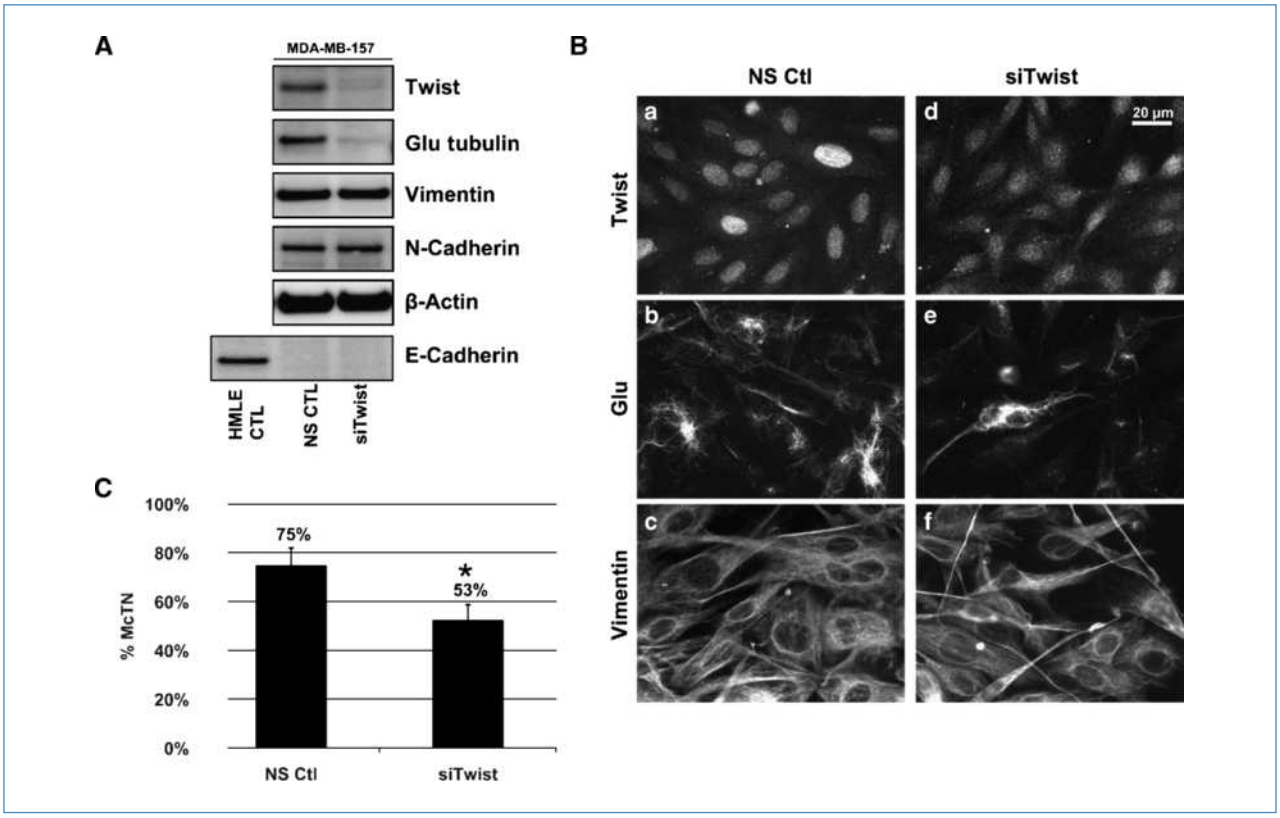

Figure 3. Endogenous Twist suppression in MDA-MB-157s decreases Glu expression and organization. A, transfection of a nonsilencing control (NS CTL) or Twist siRNA (siTwist) in MDA-MB-157s shows that suppression of Twist resulted in decreased Glu-tubulin levels. Vimentin and N-cadherin remained unchanged, and E-cadherin repression persisted. HMLE-GFP was used as a positive control for E-cadherin expression, and β-actin was used as a loading control. B, following Twist suppression in MDA-MB-157s, nuclear staining of Twist (a, d) is decreased and delocalized compared with the nonsilencing control. Twist suppression shows decreased and disrupted Glu (b, e) organization whereas vimentin (c, f) remained relatively unaffected. C, live, detached MDA-MB-157s that were scored blindly following siTwist transfection displayed significantly lower microtentacle frequencies than nonsilencing control cells. Columns, mean for six experiments, in which at least 100 CellMask-stained cells were counted; bars, SD ($P \leq 0.05$, t test, black asterisks).

previous studies showing detyrosinated tubulin enrichment that supports microtentacles, the HMLE lines were also evaluated for Glu-tubulin expression. Interestingly, the HMLE lines that expressed Twist or Snail also exhibited higher levels of Glu-tubulin that were linked to decreased expression of TTL enzyme compared with the control epithelial HMLE (Fig. 1D).

HMLE Twist and Snail have increased organization of detyrosinated microtubules

Glu-tubulin organization is a key determinant of cellular asymmetry during directional cell migration (21) and can induce abnormal cell morphology (22). We further investigated the organization of elevated Glu-tubulin in HMLE Twist and Snail lines. Immunofluorescence revealed weak cytoplasmic staining with minimal Glu-enriched microtubules in the HMLE control cell line; however, HMLE Twist and Snail cells formed an elaborate network of Glu-tubulin filaments, including extensive bundling in elongated regions of the cell (Fig. 2A).

Because microtentacles are supported by Glu-tubulin (10), we examined whether the HMLE Twist and Snail lines showed Glu-tubulin increases following detachment that could promote microtentacles (Fig. 2B). The HMLE vector control line continued to show a weak cytoplasmic staining for Glu-tubulin, consistent with the low percentage of microtentacles observed in live cell suspension. Conversely, the HMLE Twist and Snail lines displayed elevated Glu-tubulin levels throughout the cell body and microtentacles. Confocal imaging of suspended cells shows that the microtubule network remains detectable and contains a subpopulation of Glu-microtubules that can extend into the microtentacles (Supplementary Fig. S1).

Suppressing endogenous expression of Twist in MDA-MB-157 reduces detyrosinated microtubule organization and microtentacle occurrence

Given the striking increase in Glu-microtubule organization following EMT, we examined the reverse effect of suppressing endogenous Twist on cytoskeletal morphology. We targeted Twist based on epistasis experiments illustrating that Twist acts upstream of Snail (23). The MDA-MB-157 cell line was selected because it originated from a metastatic carcinoma, exhibits high *Twist* mRNA levels (ref. 24; data not shown), and displays a BasalB/mesenchymal phenotype

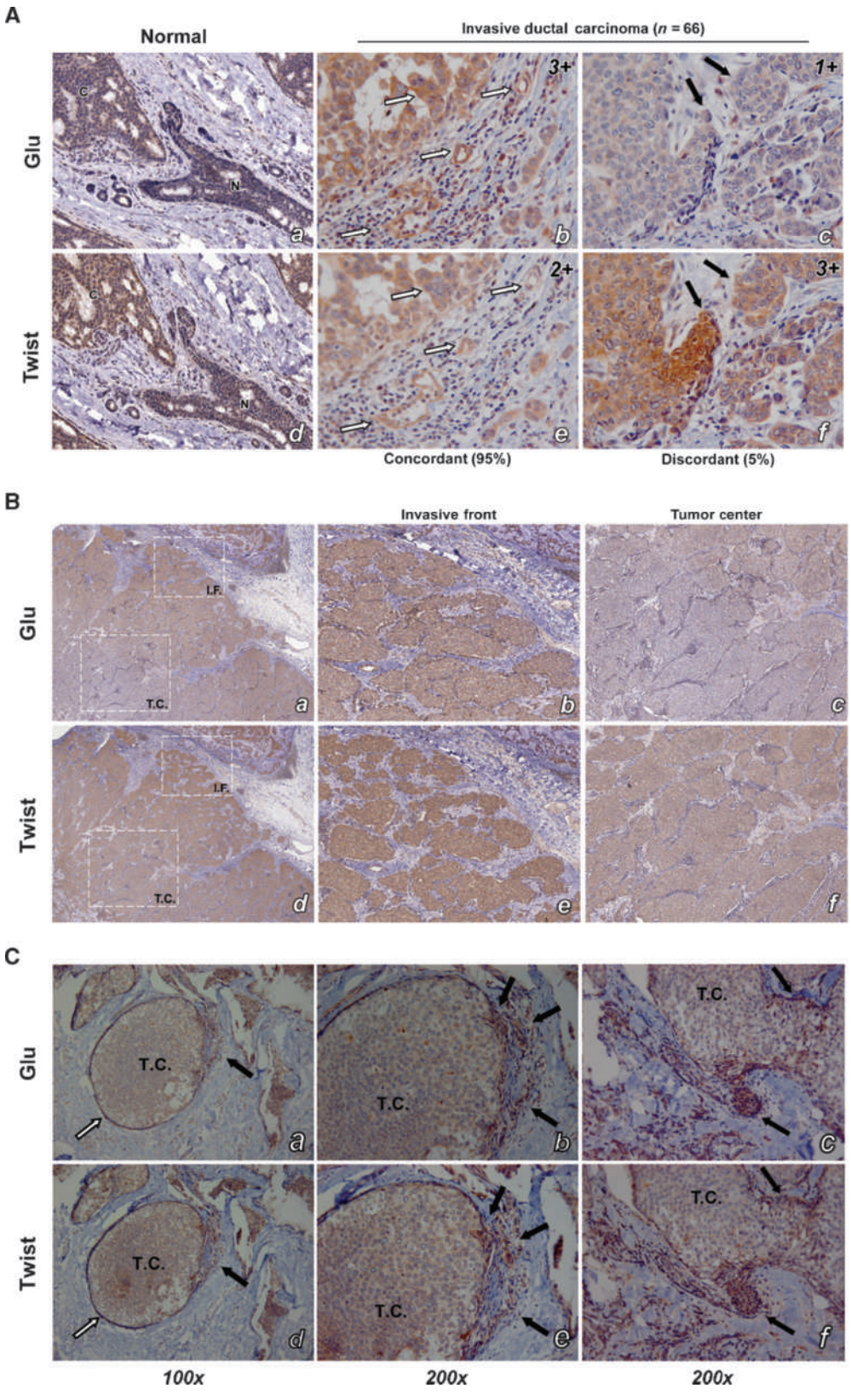
A
Normal
Invasive ductal carcinoma (n = 66)
Glu
Twist
3+
1+
2+
3+
C
N
a
b
c
d
e
f
Concordant (95%)
Discordant (5%)
B
Invasive front
Tumor center
I.F.
T.C.
C
T.C.
100x
200x
200x

(ref. 9; Supplementary Fig. S2). In addition, MDA-MB-157s displayed the highest level of microtentacles among a panel of breast carcinomas (10). Immunofluorescence also confirms that MDA-MB-157s have elevated Glu-tubulin and microtentacles containing Glu-tubulin (Supplementary Fig. S1).

MDA-MB-157s were transfected with Twist siRNA and evaluated after 4 days. Western blot analysis showed a significant decrease in Twist expression compared with the nonsilencing control siRNA (Fig. 3A). Notably, Glu-tubulin expression levels also decreased when endogenous Twist was suppressed. Other EMT hallmarks were unaffected, suggesting that Twist suppression alone did not invoke reversion to an epithelial state through mesenchymal-to-epithelial transition. This further indicates that Glu-tubulin is an early target in the Twist pathway, occurring upstream of events such as reinstatement of E-cadherin and downregulation of vimentin when EMT-associated transcription factors are suppressed (25).

Glu-tubulin organization was also altered when Twist was silenced in MDA-MB-157s. The characteristic nuclear localization of the Twist transcription factor was decreased and delocalized after 4 days of Twist siRNA, compared with a nonsilencing control (Fig. 3B, a and d). MDA-MB-157s display filamentous networks of Glu-microtubules, and suppression of Twist decreased filamentous Glu-tubulin likely through decreased microtubule stability (Fig. 3B, b and e). Whereas reducing endogenous Twist significantly decreased the expression and organization of Glu-tubulin in the MDA-MB-157s, vimentin seemed unaffected (Fig. 3B, c and f).

Because Glu-tubulin expression and organization decreased following Twist suppression, we investigated the effects of Twist silencing on microtentacles. MDA-MB-157s in which Twist, and subsequently Glu-tubulin, was downregulated with Twist siRNA (4 days) displayed a significantly lower frequency of microtentacles (53%) compared with control nonsilencing cells (75%), a 29% overall decrease in microtentacle occurrence (Fig. 3C).

Concordance of detyrosinated tubulin and Twist in invasive breast tumors

Given the coupling of Twist and Glu-tubulin *in vitro*, we examined patient samples on parallel tissue microarrays with serial matched core sections. Normal breast epithelial ducts stain weakly for both Twist and Glu, whereas the cancerous region invading the normal duct displayed stronger staining (Fig. 4A, a and d). Two independent tumor tissue cores from 33 patients (n = 66) with invasive ductal carcinoma (IDC) were analyzed blindly for Twist and Glu staining. A significant majority of IDC samples displayed similar staining intensities for Glu and Twist, and the concordance between Glu and Twist (measured as ±1 histologic scores) accounted for 95% of the IDC samples (63 of 66). Further examination revealed that the same cells within the serial sections stained for both Glu and Twist (Fig. 4A, b and e; white arrows). When staining intensity differed by at least two histologic scores (0–2 or 1–3) or within different cells, the sample was scored as "discordant" (Fig. 4A, c and f; black arrows), and was only observed in 5% of the IDC samples (3 of 66). There were varying staining intensities noted between different cores from the same patient, indicating heterogeneity of Twist and Glu expression within a given tumor. Tumor heterogeneity has implicated the surrounding microenvironment itself as an essential regulatory mechanism for EMT (2).

To examine the tumor microenvironment more extensively, larger sections of breast tumors, including adjoining normal tissue, were obtained from the UMGCC tissue repository. Low magnification revealed that both Twist and Glu stained heavily at the invasive tumor front flanking normal stroma (Fig. 4B, a and d). Higher magnification showed strong staining of the invasive front (Fig. 4B, b and e) compared with the tumor center that displayed weak staining in both Glu and Twist (Fig. 4B, c and f). Tumor sections from patients with ductal carcinoma *in situ* establish that Twist and Glu are coordinately upregulated at the earliest stages of invasion at the tumor front (Fig. 4C, black arrows). Conversely, in the later stages of tumor invasion, tumor cells that remain together as "nests" suppress both Twist and Glu (Supplementary Fig. S3).

EMT transition promotes cell reattachment

We compared the reattachment efficiency of HMLE cells to those expressing Twist or Snail using real-time electrical impedance monitoring as well as fluorescent detection over a confluent endothelial layer. The detailed impedance time course (26) shows that HMLE Twist and Snail cells attached at significantly faster rates than the HMLE vector control line (Fig. 5A; Supplementary Fig. S4). Most strikingly, HMLE-Twist reattached 8-fold more than HMLE vector control cells at 30 minutes.

HMLE variants stained with calcein-AM were also analyzed during reattachment to confluent monolayers of HBME cells (Fig. 5B). The HMLE Twist and Snail again reattached more efficiently than vector control cells ($P \leq 0.005$; n = 8;

Figure 4. Immunohistochemical staining shows high concordance between Twist and Glu expression in patient tumor samples (33 patients, 66 samples). A, duplicate tissue microarrays that stained for Glu and Twist were scored by intensity (negative, 0; weak, 1; moderate, 2; and strong, 3). Normal breast epithelial ducts (N) stain weakly for both Twist and Glu whereas the cancerous region (C) stains strongly (a, d). Patients with IDC exhibited high concordance (95%) between staining intensity and localization of Twist and Glu expression (b, e; white arrows). Discordance was observed in only 5% of patient samples (c, f; black arrows). Representative immunohistochemical scores are displayed in the top right corner. B, low magnification shows an increase in staining intensity of Twist and Glu at the invasive front (I.F.) compared with the tumor center (T.C.; a, b). Higher magnification shows stronger staining of Twist and Glu at the invasive front (b, e) whereas the tumor center stains weaker (c, f). C, ductal carcinoma *in situ* samples (a, b) show weak expression of Twist and Glu in the tumor center enclosed by the basement membrane (white arrows), but that both Twist and Glu are coordinately upregulated at sites of tumor invasion where the basement membrane is compromised (black arrows). Higher-magnification image pairs (b, e and c, f) show that Twist and Glu are upregulated in matching cells (black arrows).

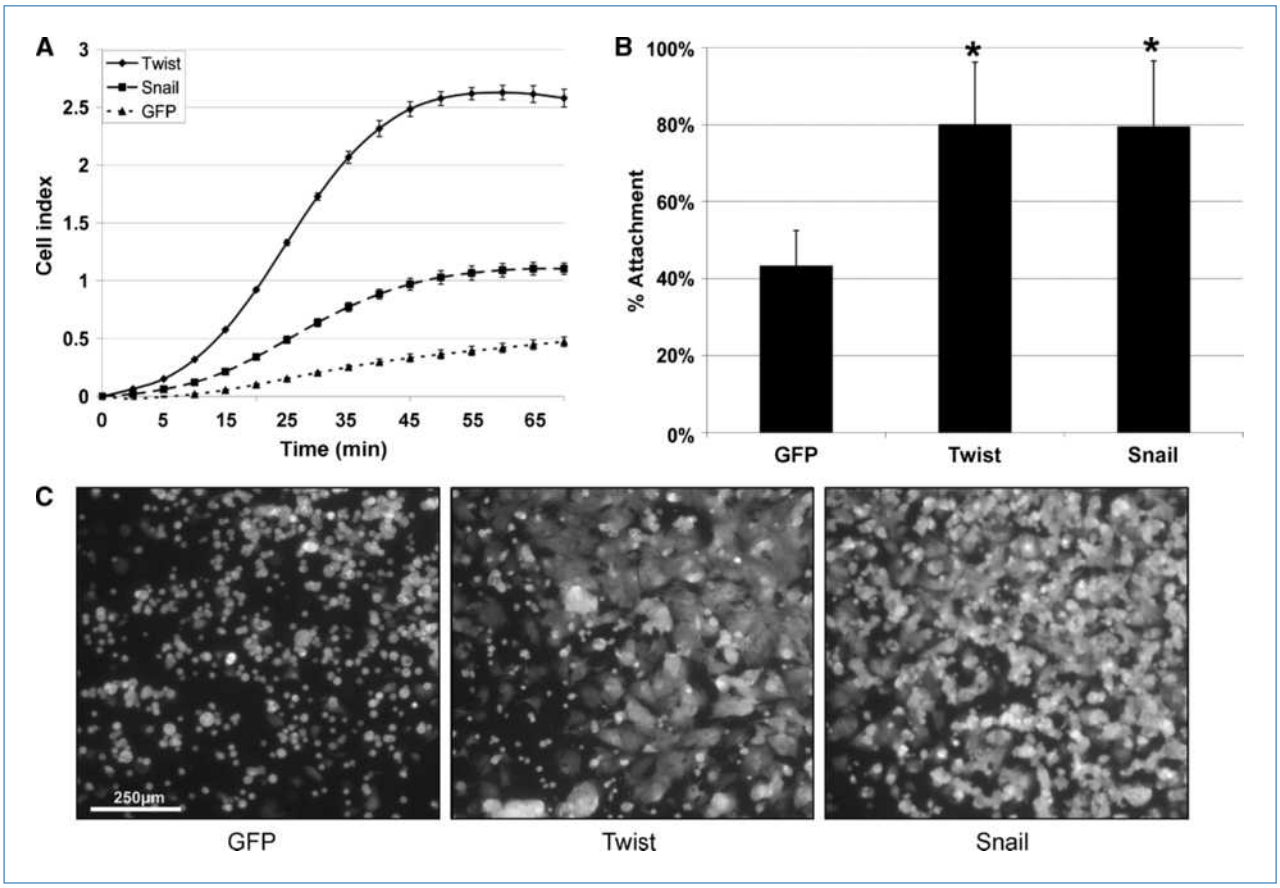

Figure 5. HMLE Twist and Snail have increased reattachment rates. A, HMLE Twist (—◆—) and Snail (- ■ -) lines attached at significantly faster rates than the HMLE-GFP (- ▲ -), as gauged by electrical impedance expressed as increasing cell index. Lines, mean for three triplicate wells; bars, SD; representative graph is shown. Three independent experiments were performed (Supplementary Fig. S4). B, calceinAM-labeled HMLE Twist and Snail cells attach significantly more to confluent HBME layers at 1 h than the HMLE-GFP cells ($P \leq 0.005$; *t* test; black asterisks). Columns, mean for eight experiments; bars, SD. C, representative images of calceinAM-labeled HMLEs over confluent HBME layers.

t test). Representative images captured at 1 hour also illustrate the difference in attachment (Fig. 5C). The majority of HMLE vector control cells retained a rounded morphology, whereas the HMLE Twist and Snail showed significantly more cells attached and spread on the HBME layer.

HMLE Twist and Snail attachment is facilitated by microtentacles

To capture microtentacles during the process of attachment, GFP-Membrane transfected cells were suspended over a confluent layer of HMBEs expressing mCherry and fixed after 20 minutes. Confocal images of these early stages of endothelial attachment are presented from a top, side, and angled view to visualize microtentacle orientation (Fig. 6). HMLE vector control cells remain rounded without any observable microtentacles at all viewing angles. The top view of HMLE Twist or Snail shows numerous microtentacles protruding from the cell (white arrows). Angled and side views when the endothelial fluorescence signal is computationally removed show that microtentacles penetrate the endothelial layer to contact the underlying surface and microtentacles on the apical surface bend toward the HBME layer. Surface renderings also show specific penetrations at endothelial cell junctions (Supplementary Fig. S5). Interestingly, the distal ends of these microtentacles are rounded, and our previous research shows that this rounded end contains actin (16), similar to neurite growth cones or sites of integrin clustering (27).

Discussion

In the present study, we show that activation of the EMT program through Twist or Snail expression significantly increases α-tubulin detyrosination by downregulating TTL and alters microtubule stability and organization to promote plasma membrane microtentacles in detached cells. This mechanism extends to metastatic human breast tumor cells, where the detyrosination and reorganization of microtubules depend on endogenous Twist expression. Microtubule stability and subsequent tubulin detyrosination are more sensitive to changes in endogenous Twist expression than the more

well-known effects on vimentin and cadherin expression, indicating that microtubule alterations are a primary effect of EMT. Both tissue microarrays and larger tissue sections from breast cancer patients show that Twist expression occurs concurrently with tubulin detyrosination *in vivo*, particularly at the invasive front where tumor cells move through adjacent tissue. Microtentacles induced by Twist or Snail promote cell reattachment, and confocal microscopy shows penetration of endothelial cell layers by microtentacles. This evidence supports a model in which the EMT program, induced in malignant cells during movement through the surrounding tissue, produces specific microtubule alterations that promote microtentacles and could provide a selective advantage during metastatic tumor cell reattachment.

Normal epithelial cells have a highly structured, rigid cytoskeletal network that is incompatible with cell motility (28). Acquisition of mesenchymal features induces an elongated, front-to-back polarized morphology that supports single-cell migration (2). The dynamic cytoskeletal properties and greater deformability of transformed cells support successful metastasis (29, 30). Although actin rearrangement during EMT has been increasingly studied (28), there has been limited investigation of EMT-induced microtubule alterations. Both the mesenchymal intermediate filament vimentin and Glu-tubulin influence cell migration, promote microtentacles, and indicate poor patient prognosis (14, 31–33), presenting a compelling case to investigate microtubule alterations that occur during EMT.

Although EMT was first described in embryogenesis (34, 35), the similarities recently observed in cancer pathology (36, 37) and tumor stem cell phenotypes (19) suggest that epithelial cells possess an inherent capacity to transform in response to activating cues. Increases in Glu-enriched stable microtubules have been reported during differentiation and implicated in generating cell asymmetry to direct migration (21, 38). Interestingly, rapid Glu-tubulin accumulation has been reported during the early stages of myogenesis when cultured myoblasts are placed in differentiation medium (39). Inhibition of tubulin detyrosination prevented morphogenesis (40), suggesting a Glu-dependent mechanism for morphologic transformations. Additionally, tubulin detyrosination in TTL-deficient cells yielded morphologic perturbations, producing large membrane extensions in adherent cells and abnormalities in cell polarization (22). Although such morphologic changes are required for development, they are potentially detrimental to cancer patients. Stabilization of microtubules, which elevates tubulin detyrosination (41), is regulated by factors such as microtubule-associated proteins (MAP) or plus-end-binding proteins such as CLIP-170, EB1, and Cap-Gly (22, 42). The tubulin

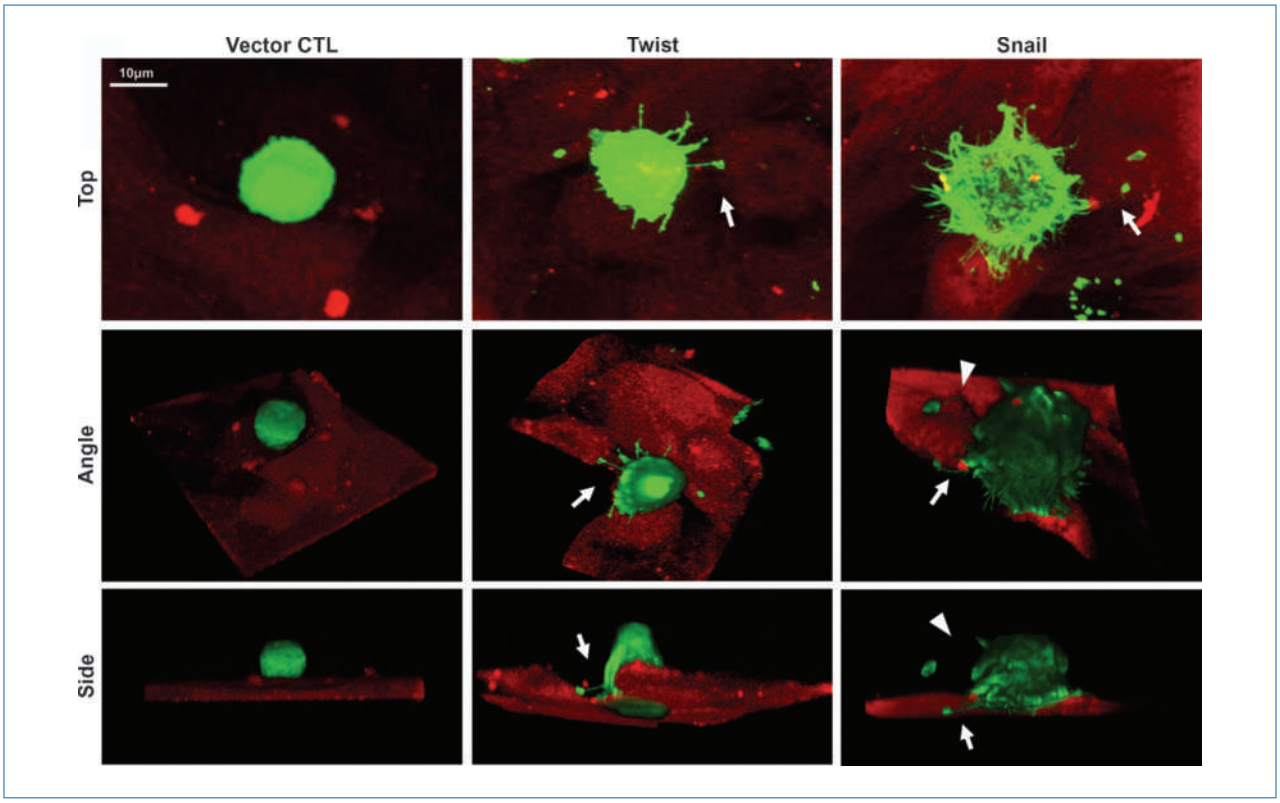

Figure 6. Microtentacles facilitate HMLE-endothelial attachment. Confocal imaging of GFP-Membrane transfected HMLE cells suspended for 20 min over a confluent layer of mCherry-labeled HBME. Top, angle, and side views of HMLE cells at the early stages of attachment show HMLE-GFP vector control cells rounded without observable microtentacles. HMLE-Twist displays a microtentacle anchoring to the top of the HBME (white arrow). HMLE-Snail exhibits microtentacles extending under (white arrow) or bending toward (white arrowheads) the HBME layer.

tyrosination/detyrosination cycle occurs through the interchange of an unidentified tubulin carboxypeptidase (TCP) that enzymatically removes the carboxyl-terminal tyrosine residue of α-tubulin, exposing a glutamate (Glu), and TTL that reincorporates the tyrosine residue (43–46). Our laboratory recently showed that metastatic breast cancers express the microtubule-stabilizing MAP protein Tau, which induces microtentacles, increases reattachment of suspended cells, and retention of CTCs in lung capillaries (47). Accumulating evidence also shows that increased persistence and stability of detyrosinated microtubules could contribute to tumor metastasis. Suppression of TTL frequently occurs during tumor progression and the accumulation of Glu-tubulin predicts tumor aggressiveness (13, 14, 32, 33). Additional investigations demonstrating increased persistence and growth of microtubules at the membrane in TTL-deficient cells (12), destabilization of cortical actin during an EMT (28), and compensatory rearrangements of stabilized microtubules after F-actin architecture is compromised (17), support an important cytoskeletal interplay that could contribute to tubulin detyrosination, microtentacle formation, and cancer invasiveness. Therefore, both TTL and TCP have become attractive therapeutic targets due to the connection between microtubule stability and carcinogenesis. Our present data show that EMT alters microtubules by downregulating TTL, increasing Glu-tubulin levels of stabilized microtubules. Testing how EMT affects the TCP enzyme is currently unfeasible because the *TCP* gene remains unidentified despite more than 30 years of studies.

The selective advantage that EMT could provide cancer cells once disseminated into the lymphatics or bloodstream is of significant interest. Although Twist suppression in highly metastatic 4T1 cells did not affect primary tumor formation, it significantly reduced the presence of tumor cells in the bloodstream, ultimately reducing the formation of metastatic lung nodules (18). Together with pathology studies showing Twist expression to be highest at invasive tumor fronts (48–50), these data suggest that Twist promotes invasion into the stroma surrounding the primary tumor but is not required for tumor growth. Our clinical data illustrate a high concordance of Twist and Glu-tubulin localization in human IDCs with the strongest expression at the invasive front, supporting a functional link between EMT and microtubule stabilization. Confocal imaging data that tubulin-based microtentacles penetrate endothelial layers during HMLE reattachment provide a mechanism to explain the *in vivo* findings that CTC reattachment is inhibited by targeting tubulin polymerization (8).

The data presented here support a novel model in which EMT suppresses TTL and promotes microtubule stability, resulting in tubulin detyrosination and the formation of microtentacles that support endothelial attachment. Cancer cells could exploit this EMT-mediated microtubule stabilization during escape from the primary tumor and subsequent invasion through the surrounding stroma. Because tumor cells can arrive in distant tissues within minutes of being released from the primary site, even transient changes in microtubule stability at the invasive front could significantly affect metastatic efficiency. This model is reinforced by the observations that CTCs depend on microtubules to attach on blood vessel walls (8) and our findings here that tubulin microtentacles promote endothelial penetration and tumor cell reattachment. Given the role of detyrosinated tubulin in cell motility and orientation, the EMT-induced microtubule alterations we report may occur as part of an inherent program for cell movement during development, but one that also primes tumor cells for metastatic success by stabilizing microtubules and promoting microtentacles.

Disclosure of Potential Conflicts of Interest

No potential conflicts of interest were disclosed.

Grant Support

R01-CA124704 from the National Cancer Institute, Breast Cancer Idea Award from USA Medical Research and Materiel Command (BC061047), and a Komen investigator-initiated research grant (KG100240).

The costs of publication of this article were defrayed in part by the payment of page charges. This article must therefore be hereby marked *advertisement* in accordance with 18 U.S.C. Section 1734 solely to indicate this fact.

Received 05/06/2010; revised 07/12/2010; accepted 08/12/2010; published OnlineFirst 10/05/2010.

References

1. Hugo H, Ackland ML, Blick T, et al. Epithelial-mesenchymal and mesenchymal-epithelial transitions in carcinoma progression. J Cell Physiol 2007;213:374–83.
2. De Wever O, Pauwels P, De Craene B, et al. Molecular and pathological signatures of epithelial-mesenchymal transitions at the cancer invasion front. Histochem Cell Biol 2008;130:481–94.
3. Polyak K, Weinberg RA. Transitions between epithelial and mesenchymal states: acquisition of malignant and stem cell traits. Nat Rev Cancer 2009;9:265–73.
4. Kalluri R, Weinberg RA. The basics of epithelial-mesenchymal transition. J Clin Invest 2009;119:1420–8.
5. Chiang AC, Massague J. Molecular basis of metastasis. N Engl J Med 2008;359:2814–23.
6. Condeelis J, Segall JE. Intravital imaging of cell movement in tumours. Nat Rev Cancer 2003;3:921–30.
7. Kedrin D, Gligorijevic B, Wyckoff J, et al. Intravital imaging of metastatic behavior through a mammary imaging window. Nat Methods 2008;5:1019–21.
8. Korb T, Schluter K, Enns A, et al. Integrity of actin fibers and microtubules influences metastatic tumor cell adhesion. Exp Cell Res 2004;299:236–47.
9. Neve RM, Chin K, Fridlyand J, et al. A collection of breast cancer cell lines for the study of functionally distinct cancer subtypes. Cancer Cell 2006;10:515–27.
10. Whipple RA, Balzer EM, Cho EH, Matrone MA, Yoon JR, Martin SS. Vimentin filaments support extension of tubulin-based microtentacles in detached breast tumor cells. Cancer Res 2008;68:5678–88.
11. Webster DR, Gundersen GG, Bulinski JC, Borisy GG. Differential turnover of tyrosinated and detyrosinated microtubules. Proc Natl Acad Sci U S A 1987;84:9040–4.
12. Peris L, Wagenbach M, Lafanechere L, et al. Motor-dependent

microtubule disassembly driven by tubulin tyrosination. J Cell Biol 2009;185:1159–66.
13. Lafanechere L, Courtay-Cahen C, Kawakami T, et al. Suppression of tubulin tyrosine ligase during tumor growth. J Cell Sci 1998;111: 171–81.
14. Mialhe A, Lafanechere L, Treilleux I, et al. Tubulin detyrosination is a frequent occurrence in breast cancers of poor prognosis. Cancer Res 2001;61:5024–7.
15. Yamaguchi H, Pixley F, Condeelis J. Invadopodia and podosomes in tumor invasion. Eur J Cell Biol 2006;85:213–8.
16. Whipple RA, Cheung AM, Martin SS. Detyrosinated microtubule protrusions in suspended mammary epithelial cells promote reattachment. Exp Cell Res 2007;313:1326–36.
17. Balzer EM, Whipple RA, Cho EH, Matrone MA, Martin SS. Antimitotic chemotherapeutics promote adhesive responses in detached and circulating tumor cells. Breast Cancer Res Treat 2010;121:65–78.
18. Yang J, Mani SA, Donaher JL, et al. Twist, a master regulator of morphogenesis, plays an essential role in tumor metastasis. Cell 2004;117:927–39.
19. Mani SA, Guo W, Liao MJ, et al. The epithelial-mesenchymal transition generates cells with properties of stem cells. Cell 2008;133: 704–15.
20. Elenbaas B, Spirio L, Koerner F, et al. Human breast cancer cells generated by oncogenic transformation of primary mammary epithelial cells. Genes Dev 2001;15:50–65.
21. Gundersen GG, Bulinski JC. Selective stabilization of microtubules oriented toward the direction of cell migration. Proc Natl Acad Sci U S A 1988;85:5946–50.
22. Peris L, Thery M, Faure J, et al. Tubulin tyrosination is a major factor affecting the recruitment of CAP-Gly proteins at microtubule plus ends. J Cell Biol 2006;174:839–49.
23. Smit MA, Geiger TR, Song JY, Gitelman I, Peeper DS. A Twist-Snail axis critical for TrkB-induced EMT-like transformation, anoikis resistance and metastasis. Mol Cell Biol 2009;29:3722–37.
24. Blick T, Widodo E, Hugo H, et al. Epithelial mesenchymal transition traits in human breast cancer cell lines. Clin Exp Metastasis 2008;25: 629–42.
25. Kwok WK, Ling MT, Lee TW, et al. Up-regulation of TWIST in prostate cancer and its implication as a therapeutic target. Cancer Res 2005;65:5153–62.
26. Atienza JM, Yu N, Kirstein SL, et al. Dynamic and label-free cell-based assays using the real-time cell electronic sensing system. Assay Drug Dev Technol 2006;4:597–607.
27. Lowery LA, Van Vactor D. The trip of the tip: understanding the growth cone machinery. Nat Rev Mol Cell Biol 2009;10:332–43.
28. Yilmaz M, Christofori G. EMT, the cytoskeleton, and cancer cell invasion. Cancer Metastasis Rev 2009;28:15–33.
29. Raz A, Geiger B. Altered organization of cell-substrate contacts and membrane-associated cytoskeleton in tumor cell variants exhibiting different metastatic capabilities. Cancer Res 1982;42: 5183–90.
30. Guck J, Schinkinger S, Lincoln B, et al. Optical deformability as an inherent cell marker for testing malignant transformation and metastatic competence. Biophys J 2005;88:3689–98.
31. Domagala W, Lasota J, Dukowicz A, et al. Vimentin expression appears to be associated with poor prognosis in node-negative ductal NOS breast carcinomas. Am J Pathol 1990;137:1299–304.
32. Soucek K, Kamaid A, Phung AD, et al. Normal and prostate cancer cells display distinct molecular profiles of α-tubulin posttranslational modifications. Prostate 2006;66:954–65.
33. Kato C, Miyazaki K, Nakagawa A, et al. Low expression of human tubulin tyrosine ligase and suppressed tubulin tyrosination/detyrosination cycle are associated with impaired neuronal differentiation in neuroblastomas with poor prognosis. Int J Cancer 2004;112:365–75.
34. Hay ED. An overview of epithelio-mesenchymal transformation. Acta Anat (Basel) 1995;154:8–20.
35. Hay ED. The mesenchymal cell, its role in the embryo, and the remarkable signaling mechanisms that create it. Dev Dyn 2005;233: 706–20.
36. Guarino M, Rubino B, Ballabio G. The role of epithelial-mesenchymal transition in cancer pathology. Pathology 2007;39:305–18.
37. Yang J, Weinberg RA. Epithelial-mesenchymal transition: at the crossroads of development and tumor metastasis. Dev Cell 2008; 14:818–29.
38. Onishi K, Higuchi M, Asakura T, Masuyama N, Gotoh Y. The PI3K-Akt pathway promotes microtubule stabilization in migrating fibroblasts. Genes Cells 2007;12:535–46.
39. Gundersen GG, Khawaja S, Bulinski JC. Generation of a stable, post-translationally modified microtubule array is an early event in myogenic differentiation. J Cell Biol 1989;109:2275–88.
40. Chang W, Webster DR, Salam AA, et al. Alteration of the C-terminal amino acid of tubulin specifically inhibits myogenic differentiation. J Biol Chem 2002;277:30690–8.
41. Webster DR, Gundersen GG, Bulinski JC, Borisy GG. Assembly and turnover of detyrosinated tubulin *in vivo*. J Cell Biol 1987;105: 265–76.
42. Zhang T, Zaal KJ, Sheridan J, Mehta A, Gundersen GG, Ralston E. Microtubule plus-end binding protein EB1 is necessary for muscle cell differentiation, elongation and fusion. J Cell Sci 2009;122: 1401–9.
43. Gundersen GG, Khawaja S, Bulinski JC. Postpolymerization detyrosination of α-tubulin: a mechanism for subcellular differentiation of microtubules. J Cell Biol 1987;105:251–64.
44. Webster DR, Modesti NM, Bulinski JC. Regulation of cytoplasmic tubulin carboxypeptidase activity during neural and muscle differentiation: characterization using a microtubule-based assay. Biochemistry 1992;31:5849–56.
45. Wehland J, Weber K. Turnover of the carboxy-terminal tyrosine of α-tubulin and means of reaching elevated levels of detyrosination in living cells. J Cell Sci 1987;88:185–203.
46. Barra HS, Arce CA, Argarana CE. Posttranslational tyrosination/detyrosination of tubulin. Mol Neurobiol 1988;2:133–53.
47. Matrone MA, Whipple RA, Thompson K, et al. Metastatic breast tumors express increased tau, which promotes microtentacle formation and the reattachment of detached breast tumor cells. Oncogene 2009;29:3217–27.
48. Fendrich V, Waldmann J, Feldmann G, et al. Unique expression pattern of the EMT markers Snail, Twist and E-cadherin in benign and malignant parathyroid neoplasia. Eur J Endocrinol 2009;160: 695–703.
49. Usami Y, Satake S, Nakayama F, et al. Snail-associated epithelial-mesenchymal transition promotes oesophageal squamous cell carcinoma motility and progression. J Pathol 2008;215:330–9.
50. Hlubek F, Brabletz T, Budczies J, Pfeiffer S, Jung A, Kirchner T. Heterogeneous expression of Wnt/β-catenin target genes within colorectal cancer. Int J Cancer 2007;121:1941–8.